Fullertubes Inhibit Mycobacterial Viability and Prevent Biofilm Formation by Disrupting the Cell Wall

Shenoy, V[1,2]., Gunda, R[1]., Noble, C[2]., Haraguchi, A[1]., Stevenson, S[2]., and Daniel, J[1*]

[1]Department of Biological Sciences, Purdue University Fort Wayne, Fort Wayne, IN 46805, United States of America

[2]Department of Chemistry and Biochemistry, Purdue University Fort Wayne, Fort Wayne, IN 46805, United States of America

*Address for correspondence:
Jaiyanth Daniel, Ph.D.
Associate Professor,
Department of Biological Sciences
Purdue University Fort Wayne
SB 380, 2101 E Coliseum Blvd.,
Fort Wayne, IN 46805
Phone: 260-481-5703
Email: danielj@pfw.edu
Fax: 260-481-6087

Short title: Fullertube disruption of mycobacterial cell wall

Abstract

Mycobacterium tuberculosis and nontuberculous mycobacteria such as *Mycobacterium abscessus* cause diseases that are becoming increasingly difficult to treat due to emerging antibiotic resistance. The development of new antimicrobial molecules is vital for combating these pathogens. Carbon nanomaterials (CNMs) are a class of carbon-containing nanoparticles with promising antimicrobial effects. Fullertubes (C_{90}) are novel carbon allotropes with a structure unique among CNMs. The effects of fullertubes on any living cell have not been studied. In this study, we demonstrate that pristine fullertube dispersions show antimicrobial effects on *Mycobacterium smegmatis* and *M. abscessus*. Using scanning electron microscopy, light microscopy and molecular probes, we investigated the effects of these CNMs on mycobacterial cell viability, cellular integrity and biofilm formation. C_{90} fullertubes at 1 µM inhibited mycobacterial viability by 97 %. Scanning electron microscopy revealed that the cell wall structure of *M. smegmatis* and *M. abscessus* was severely damaged within 24 h of exposure to fullertubes. Additionally, exposure to fullertubes nearly abrogated the acid-fast staining property of *M. smegmatis*. Using SYTO-9 and propidium iodide, we show that exposure to the novel fullertubes compromises the integrity of the mycobacterial cell. We also show that the permeability of the mycobacterial cell wall was increased after exposure to fullertubes from our assays utilizing the molecular probe dichlorofluorescein and ethidium bromide transport. C_{90} fullertubes at 0.37 µM and C_{60} fullerenes at 0.56 µM inhibited pellicle biofilm formation by 70% and 90%, respectively. This is the first report on the anti-mycobacterial activities of fullertubes and fullerenes.

Keywords: Fullertubes; fullerenes; mycobacteria; cell wall; biofilm

SIGNIFICANCE STATEMENT

The recently isolated fullertubes (C_{90}) are carbon nanoparticles with tubular molecular structures and hemispherical end caps and their effects on any living cell have not been investigated. We show that the novel fullertubes inhibit mycobacterial cell growth and cause physical damage to the cell envelope in *Mycobacterium smegmatis* and in *Mycobacterium abscessus*, an infectious organism of clinical importance. We also show that fullertubes and fullerenes inhibit biofilm formation which is a key phenotype of mycobacterial pathogenesis.

1.Introduction

The genus *Mycobacterium* contains many notable pathogenic species, including *Mycobacterium tuberculosis* (Mtb) *and Mycobacterium abscessus* (Mab). Mtb is the causative agent of tuberculosis, a disease that is particularly difficult to treat due to its ability to develop antibiotic tolerance (1). Mab is emerging as a public health threat since it has been causing increasing numbers of infections in the United States and globally and is highly antibiotic-resistant (2). Research and development of novel antimicrobial agents against these organisms is greatly needed.

Carbon nanomaterials (CNMs), as a class of molecules, contain diverse compounds, including carbon nanotubes, graphene oxide particles, fullerene, and fullertubes. Many of these compounds have been shown to possess antibacterial effects (3). The antibacterial effects of CNMs with different dimensionalities have been attributed, among several possibilities, to physical damage of the bacterial cell wall, ROS-dependent and ROS-independent oxidative stress and the ability of CNMs to penetrate into and extract the phospholipids from the bacterial lipid membranes (4). Buckminster fullerenes (C_{60}) are a well-investigated class of carbon allotropes with a characteristic spherical shape. The antibacterial effects of fullerenes against Gram-positive and Gram-negative bacteria have been investigated (5). CNMs are reported to be environmentally benign and useful as antibacterial food packaging materials (6). A recent report described the antibacterial activity of water-soluble fullerene against Gram-positive and Gram-negative bacteria. This report also showed that fullerenes penetrate eukaryotic cells by endocytosis but that the toxicity was limited (7).

Fullertubes (C_{90}) are a class of recently isolated compounds with a hybrid structure of fullerenes and carbon nanotubes (8). Fullertubes contain the hexagonal-patterned body of a carbon nanotube with end caps that resemble one half of a fullerene. As a result of their hybrid structure, they possess unique chemical properties (9). The effects of fullertubes on any living cell have not been investigated. In this study, we use well-agitated fullertube and fullerene dispersions in a 1:3 (v/v) mixture of oleic acid:dimethyl sulfoxide (DMSO), a novel preparation medium utilized to maintain the retention of fullertubes and fullerenes in the dispersion and minimize preparation loss of the fullertubes that are not available commercially. Earlier studies have primarily used fullerenes (C_{60}) in different preparations or functionalized forms (10). C_{70}, a compound with a structure similar to C_{60}, has also been studied to a lesser extent (11). However, there are no reports on the effects of fullertubes and fullerenes in mycobacteria.

In this study, we exposed *Mycobacterium smegmatis* (Msm) and *M. abscessus* (Mab) cells to fullertubes (C_{90}) and fullerenes (C_{60}) to investigate their effects. We found that fullertubes and fullerenes decrease cellular viability in Msm and Mab. We additionally demonstrate, using scanning electron microscopy (SEM) and acid-fast staining microscopy, that fullertubes and fullerenes damage the mycobacterial cellular envelope. Furthermore, using multiple molecular probes, we show that fullertubes and fullerenes permeabilize the mycobacterial cell wall and damage the cell envelope. We also demonstrate that fullertubes and fullerenes inhibit biofilm formation in *M. smegmatis*.

2. Materials and Methods

2.1 Mycobacterial growth conditions

Mycobacterium smegmatis mc²155 and *Mycobacterium abscessus* ATCC 19977 (ATCC, Manassas, VA) were maintained as glycerol stocks at - 80 °C. The bacteria were grown in Middlebrook 7H9 medium (with 0.05 % Tween 80) + 10 % (v/v) Middlebrook oleic acid albumin dextrose catalase (OADC) enrichment with shaking at 37 °C till the cultures reached mid-log phase (optical density at 600 nm [OD_{600}] ~ 0.6) and used in assays as described below.

2.2 Preparation and characterization of fullerene and fullertube dispersions

Fullertubes (C_{90}-D_{5h}) were purified as described earlier (8). Fullerenes (C_{60}-I_h) were obtained from MER Corp., Tucson, AZ. Dispersions of fullertubes and fullerenes were prepared as follows: 1 mg of the respective fullertube or fullerene was first dissolved in 10 mL of chloroform. Oleic acid (0.25 mL) was then added and mixed thoroughly. After evaporation of the chloroform in a water bath at 50 °C under a stream of nitrogen, the suspension was transferred to a glass tube and sterilized by autoclaving (121 °C, 20 min). After cooling, 0.75 mL of dimethyl sulfoxide (DMSO, 0.2 µm filter-sterilized) was added aseptically. All assays were performed using these 1 mg/mL stock dispersions of the respective fullertube or fullerene in oleic acid:DMSO (1:3, v/v). The particle size distributions for the C_{60} dispersion were determined by dynamic light scattering (DLS) analysis of a 10 µg/mL C_{60} dispersion made in oleic acid:DMSO (1:3, v/v) at a pH of 6.72. Measurements were performed on a Zetasizer-Nano ZS90 (Malvern Panalytical, Malvern, UK) in disposable DTS001 polystyrene cuvettes (Malvern Panalytical, Malvern, UK), at 25 °C. The standard Zetasizer protocol for fullerene nanoparticles was followed, with the dispersant refractive index and viscosity set to 1.474 and 2.0 cP, respectively, to reflect the approximate values for the oleic acid:DMSO (1:3, v/v) dispersant.

2.3 Antimicrobial activity determination

M. smegmatis and *M. abscessus* cells grown to mid log-phase were diluted to approximately 5 x 10^4 CFUs/mL and were then exposed to dispersions of C_{60} at final concentrations of 0.1 µg/mL, 0.2 µg/mL, 0.5 µg/mL, and 1.0 µg/mL or C_{90} at final concentrations of 0.2 µg/mL and 1.0 µg/mL. Appropriate dilutions of the fullertube/ fullerene dispersions were added. Negative (dispersant) control cells were exposed to the same respective volumes of the 1:3 (v/v) oleic acid:DMSO dispersant. The maximum final concentration of oleic acid was limited to 0.1 % (v/v).

The bacteria were then incubated with shaking at 37 °C for nearly 40 h (*M. smegmatis*) or for about 205 h (*M. abscessus*) until the cells exposed to the dispersant control reached an OD_{600} of 0.7-0.8. The cell cultures were then serially-diluted with thorough vortexing and sonication for 1 min for each dilution step in a Branson 2510 water bath sonicator (100 W output; Branson Ultrasonics Corporation, Danbury, CT) to disperse clumps of cells. The colony-forming units (CFUs) were determined after appropriate serial dilution and agar plating. The colonies on the agar plates were counted after 3 days (*M. smegmatis*) or 4 days (*M. abscessus*).

2.4 Scanning electron microscopy preparation and imaging

M. smegmatis and *M. abscessus* cells at mid log-phase were diluted to 10^4 CFUs/mL and exposed to the fullertube or fullerene dispersions at final concentrations of 0.2 µg/mL or the oleic acid:DMSO control (0.1 % v/v final concentration) with shaking at 37 °C. *M. smegmatis* cells were collected after 2 h and 24 h incubation with the CNMs and *M. abscessus* cells were collected after 24 h of incubation. The bacterial samples were then prepared for scanning electron microscopy imaging following a slightly modified version of a protocol described earlier (12). Briefly, the cells were retained on a 0.22-micron polycarbonate filter and were fixed in a solution of 4 % (v/v) formaldehyde in 0.1 M phosphate buffer, pH 7.4 for 2.5 h, dehydrated through a graded ethanol series consisting of dehydration by 30 %, 50 %, 70 %, and 100 % ethanol in water solutions, with the 100 % ethanol dehydration step being performed twice (12, 13). The filters were then removed from their housings and then further dried using the t-butanol drying procedure as described earlier (14). The samples were immersed in t-butanol and cooled at 4 °C until frozen. The t-butanol was then sublimated at a pressure range of approximately 50 mTor for 2 h, in a vacuum desiccator connected to a rotary pump. The samples were then sputter-coated with gold at a thickness of 2 nm using a Quorum Q150T sample coater (Quorum Technologies, East Sussex, UK). The samples were then imaged at a voltage of 3.00 kV and a magnification of 15,000X using a Hitachi S3400N (Hitachi High Technologies, Tokyo, Japan) scanning electron microscope.

2.5 Acid-fast staining and microscopy

M. smegmatis and *M. abscessus* cells were grown to mid log-phase, diluted to 10^4 CFUs/mL and exposed to either the C_{90} or C_{60} dispersions at a concentration of 0.2 µg/mL or the oleic acid:DMSO control (0.1 % v/v final concentration). The cells were then incubated at 37 °C for 24 hours with shaking. Cells were then collected by centrifugation and resuspended in 1 mL sterile

culture medium. The cells were then pelleted once again and resuspended in 50 µL of sterile medium. The resuspended cells were spread on glass slides, air dried and heat-fixed. Samples were stained with the traditional procedure for the Ziehl-Neelsen staining and imaged under bright-field illumination using an Olympus CX22LED microscope and a Leica DFC295 camera. A total of 15 fields for each group across three independent experiments were captured.

2.6 SYTO-9/ Propidium Iodide staining for cell envelope integrity

We adapted the procedure detailed in an earlier study to probe the envelope integrity of *M. smegmatis* (15). Planktonic, log-phase *M. smegmatis* cells were exposed to dispersions of C_{90} or C_{60} at final concentrations of 0.2 µg/mL or the oleic acid:DMSO control (0.02 % v/v final concentration) for 2 hours. The cells were washed with 0.85 % NaCl in ultrapure water and exposed to the 2X SYTO-9/propidium iodide solution (LIVE/DEAD *Bac*Light Bacterial Viability Kit, Molecular Probes, Invitrogen, CA, USA) and incubated at room temperature in the dark for 15 min, after which the green fluorescence (Ex. 485 nm/ Em. 528 nm) and red fluorescence (Ex. 530 nm/ Em. 590 nm) were measured using an Agilent BioTek Synergy LX Multimode Reader (Santa Clara, CA). The measured fluorescence ratio was normalized using viable cell counts (CFUs) determined by agar plating. The relative green/ red fluorescence ratios were calculated against the Msm + oleic acid:DMSO control.

2.7 Ethidium bromide transport assay

We followed a modified version of previously described protocols to monitor the accumulation and efflux of ethidium bromide (EtBr) (16, 17). *M. smegmatis* (log phase) culture was washed and resuspended in sodium phosphate buffer pH 7.4 with 0.05 % (v/v) Tween 80 (PBST) to an OD_{600} of 0.4. Then, 1 mL of the bacterial suspension was centrifuged (16,000 x g, 5 min) and the cell pellets obtained were resuspended in PBST containing 0.4 µg/mL C_{60} or C_{90} to assess the impact of fullertubes and fullerenes on the transport of EtBr into and out of the mycobacterial cell. Aliquots of 200 µL were transferred in triplicates to 96-well plates and EtBr was added to a final concentration of 1 µg/mL. The accumulation of EtBr was measured at room temperature by recording the red fluorescence values (Ex. 530 nm, Em. 590 nm) in a microplate reader Agilent BioTek Synergy LX Multimode Reader (Santa Clara, CA) over 60 min. To examine the efflux of EtBr, the cells (OD_{600} = 0.4) were incubated with 150 µg/mL verapamil (0.5X MIC) for 15 min at room temperature. Then, EtBr was added to a final concentration of 3 µg/mL and incubated for 1 h at 25 °C to promote maximum accumulation of EtBr. After

incubation, 1 mL bacterial cultures were centrifuged, washed, and cell pellets were placed on ice immediately. The cell pellets were resuspended in PBST containing 0.4 µg/mL fullertubes or fullerenes and incubated on ice for 1 h. Aliquots of 200 µL were transferred to a 96-well plate and red fluorescence was measured as described above, every 5 min for 60 min at 37 °C. In this assay, log phase cells were utilized to allow the effective detection of fluorescence signals.

2.8 Dichlorofluorescein assay of cellular reductive state

Planktonic log-phase *M. smegmatis* cells were exposed to dispersions of C_{90} or C_{60} at a final concentration of 0.2 µg/mL and the oleic acid:DMSO control (0.02 % v/v final concentration) for 2 h. The cells were then pelleted, washed with 0.85 % NaCl in ultrapure water and inoculated with dichlorodihydrofluorescein diacetate, after which the green fluorescence (Ex. 485 nm/ Em. 528 nm) was measured. The measured fluorescence intensity was normalized using viable cell counts (CFUs) determined by agar plating.

2.9 FOX II lipid peroxidation assay

Lipid peroxides were determined using the Ferrous Xylenol Orange (FOX II) assay as previously described with some modifications (18, 19). The FOX II reagent contains 90 % methanol, butylated hydroxytoluene (4.4 mM), 25 mM H_2SO_4, 250 mM ferrous ammonium sulphate, and 100 mM xylene orange. Briefly, *M. smegmatis* cells (log-phase) grown in Middlebrook 7H9 broth supplemented with 10 % (v/v) Middlebrook ADC enrichment were washed and diluted to 10^6 CFUs/mL in phosphate buffered saline containing 0.05 % Tween 80 (PBST). Then, 1 mL of the bacterial suspension was centrifuged (16,000 x g, 5 min) and the cell pellet obtained was suspended in PBST containing 0.2 and 0.4 µg/mL C_{90} or C_{60}. The samples were then incubated at 37 °C with shaking for 4 h. Following the treatment, the cells were centrifuged at 16,000 x g for 5 min and washed using PBST. The resultant cell pellet was suspended in a mixture of chloroform and methanol (1:2, v/v) and incubated for 40 min. To this, 800 µL of FOX II reagent was added and left to incubate in the dark for 30 min. 200 µL of the sample was then measured spectrophotometrically at 560 nm. The recorded absorbance values for each condition were normalized against cells treated only with the oleic acid:DMSO dispersant, which served as the control.

2.10 Fullerene/ fullertube effects on *M. smegmatis* pellicle biofilm formation

We adapted a previously described assay to measure *M. smegmatis* biofilm formation in borosilicate glass tubes (20). Pellicle formation was monitored by growing 1:100 dilution of log-phase cultures of mycobacteria without shaking in Middlebrook 7H9 medium supplemented with 2 % (v/v) Middlebrook ADC enrichment and 0.5 % glucose and lacking Tween 80 at 37 °C for 72 h. Briefly, 5 mL cultures were exposed to varying concentrations (0.2 µg/mL and 0.4 µg/mL) of fullertubes or fullerenes with oleic acid:DMSO (1:3, v/v) serving as the dispersant control. Following the incubation period to allow pellicle (floating) biofilm formation, the tubes were vortexed and the floating biofilm was collected from the glass tube by filtration on a fine-mesh nylon filter. The cells adhered together in the biofilm were separated from the planktonic cells by gently washing the biofilms retained on the fine-mesh nylon filter three times with distilled water. The biofilms were stained on the nylon filters by exposing them to 0.5 mL of 1 % (w/v) Crystal Violet solution and incubating at room temperature for 15 min. Subsequently, the Crystal Violet solution was removed and the stained biofilm on the nylon filter was washed three times with distilled water. The bound Crystal Violet was eluted from the biofilm cells using 2 mL of 95 % (v/v) ethanol. The absorbance was measured at 600 nm using a microplate reader. For the samples whose absorbance values were greater than 1.0, the eluate was diluted with 95 % (v/v) ethanol and measured again.

2.11 CNM-Isoniazid synergism and Most Probable Number assays

Planktonic log-phase *M. smegmatis* cells grown to an OD_{600} of approximately 0.7 in Middlebrook 7H9 broth with Tween 80 and 10 % OADC were exposed to dispersions of C_{90} or C_{60} at final concentrations of 0.2 µg/mL or oleic acid:DMSO (0.1 % v/v final concentration) and untreated cell controls were incubated for 2 h at 37 °C with shaking. In order to determine potential synergistic activities of CNMs with isoniazid, we selected two sub-MIC concentrations of INH that would result in countable CFUs on agar plates. These sub-MIC concentrations were selected based on previously reported MIC values for INH against *M. smegmatis* mc^2155 (21). Following CNM exposure, the samples were exposed to isoniazid at a final concentration of 2 µg/mL or 10 µg/mL at 37 °C for an additional 24 hours. Cells exposed only to oleic acid:DMSO with isoniazid at the respective concentrations were used as controls. The cells were then serially diluted 10-fold by mixing 100 µL of each cell suspension in 900 µL of Middlebrook 7H9 containing 10 % OADC. Appropriate dilutions were spread-plated onto Middlebrook 7H10 agar plates containing 10 % OADC. The plates were incubated at 37 °C for 3 days and CFUs were determined. The serially-diluted cultures were also subjected to the Most Probable Number

(MPN) assay following a modification of procedures described earlier for *M. tuberculosis* (22, 23). Briefly, 200 µL of each dilution (from 10^{-2} to 10^{-9}) in triplicate for all samples were placed in 96-well plates and incubated for 3 days at 37 °C after which cell viability was assessed by adding 25 µL of 0.02 % (w/v) resazurin and further incubation for 24 h at 37 °C. Color change from blue to pink was taken as indication of positive growth. The MPN/ mL values were determined from a standard MPN index for combinations of positive tubes in a 3-tube dilution series with appropriate adjustments for the volumes and dilutions used in our assay (24, 25).

3. Results

3.1 Fullertube and Fullerene dispersions decrease the viability of mycobacteria

We characterized the effects of the novel C_{90} fullertubes on the viability of *M. smegmatis* and *M. abscessus* cells and compared their activities with those of the C_{60} fullerenes. *M. smegmatis* was used as the primary organism in this study since it is a well-studied model organism for tuberculosis (26). We also examined the effects of the CNMs on *M. abscessus* viability since it is a nontuberculous mycobacterial pathogen. Fullertubes and fullerenes significantly decreased the measured colony forming units for both organisms. The decrease in the colony forming units showed a dependence on the concentration of the fullertubes and fullerenes (Table 1, Fig. 1 A, C). At 0.2 µg/mL, *M. smegmatis* exposed to the fullertube and fullerene dispersions showed average percent survivals of 63 % and 83 %, respectively at the indicated time-points of incubation with the CNMs, compared to the control cells exposed to oleic acid:DMSO alone. *M. smegmatis* exposed to C_{90} and C_{60} at concentrations of 1.0 µg/mL displayed a significant decrease in cell viability, with only 3 – 8 % of the cells surviving exposure to the CNMs at this concentration (Fig. 1 B). *M. abscessus* exposed to C_{90} or C_{60} also significantly reduced cell viability. Only 3 % of the *M. abscessus* cells survived exposure to C_{90} at 1.0 µg/mL while 14 % survived exposure to C_{60} at 1.0 µg/mL (Fig. 1 D). We observed that the dispersant in which the CNMs were suspended (1:3 [v/v] oleic acid:DMSO) did affect cellular viability. At the concentrations of 0.1 % (v/v) and 0.02 % (v/v), which correspond with the concentrations of CNMs used, the dispersant decreased the survival of the mycobacterial cells to 58.9 % and 87.8 % respectively (on average) compared to the untreated cells. Therefore, we used the dispersant-treated cells as the baseline control to compare the CNM-treated cells and the percent survival data in Fig. 1 are depicted relative to this control. We also investigated whether the water bath sonication procedure we followed to disperse clumps of mycobacteria prior to agar plating for CFUs affected cell viability and determined that sonication of cells did not affect cell viability (4.6 ± 0.2 CFUs/mL for unsonicated cells versus 5.4 ± 0.2 CFUs/mL for sonicated cells).

Table 1. Viability of *Mycobacterium smegmatis* exposed to C_{60} at different concentrations.

C_{60} Concentration (µg/mL)	Percent Cell Viability Avg(± SD)[c]	P-value[d]
0.1[a]	81.0 (±7.1)	0.379
0.2[b]	83.2 (±23.9)	0.376
0.5[b]	5.0 (±4.0)	< 0.01
1.0[b]	7.8 (±7.4)	< 0.01
2.0[b]	6.6 (±8.3)	< 0.01
10.0[b]	6.0 (±10.3)	< 0.01

[a]n = 2, [b]n=3. [c]Average percent survival calculated against a representative 1:3 oleic acid:DMSO controls. [d] One-way ANOVA.

3.2 *Mycobacteria* show damaged cellular morphology after exposure to fullertubes and fullerenes.

To determine the morphological effects of the prepared fullertube and fullerene dispersions, we prepared scanning electron micrographs of treated *M. smegmatis* and *M. abscessus* cells at various time points (Fig. 2). We observed that the membrane morphology of untreated *M. smegmatis* and *M. abscessus* and cells treated with the oleic acid:DMSO control showed smooth and intact cellular envelopes, consistent with the expected wild-type phenotype (2, 27-29). In contrast, the fullertube- and fullerene-treated cells showed various damaged phenotypes of varying severity. *M. smegmatis* cells exposed to fullertubes or fullerenes displayed slight signs of damage at the 2 h time point, presenting rougher membrane morphologies characterized by bumps, inclusions, and breakdowns in the cellular envelope compared to the controls (Fig. 2, top row). At the 24 h timepoint, we observed a more dramatic change in phenotype. Our observations of several microscopic fields shows that *M. smegmatis* and *M. abscessus* cells exposed to fullertubes or fullerenes for 24 h had broken cell envelopes or appeared as shriveled cells (Fig. 2, middle and bottom rows). Some of these cells also showed bumps, inclusions, and breakdowns in the cellular envelope. Additionally, fields at the 24 h timepoint contained signs of cellular debris, covering the holes in the background filter paper. While we did observe a few fields with cells containing undamaged cell envelopes in the CNM-treated samples, we did not observe any damaged phenotypes in the untreated cells or in the control cells exposed to the oleic acid:DMSO dispersant. The effects of fullertubes and fullerenes on the morphology of *M. smegmatis* were also observed in the acid-fast staining of these cells (Figure 3). Untreated cells and cells exposed to the oleic acid:DMSO control revealed smooth envelope morphologies consistently stained deep purple, as expected.

However, cells treated with fullertubes or fullerenes displayed a rough, damaged envelope morphology and a markedly lower retention of the Carbolfuchsin stain resulting in very light, purple-stained cells.

3.3 Fullertubes and fullerenes decrease the integrity and increase the permeability of the cell envelope of *Mycobacterium smegmatis*

We used fluorescent molecular probes to further characterize the molecular effects of fullertubes and fullerenes. We used the SYTO-9/ Propidium Iodide (PI) fluorescent probes to assess the cell envelope integrity of *M. smegmatis* cells exposed to fullertubes or fullerenes (Figure 4 A). SYTO-9 is a membrane-permeable DNA-binding fluorescent probe that enters all cells to intercalate with cellular DNA and fluoresces green (15). PI preferentially enters cells with damaged membranes or show increased permeability to polar compounds. When PI enters the cell, it can also intercalate with intracellular DNA and fluoresce red. When used simultaneously, the red fluorescence of PI quenches the green fluorescence of SYTO-9 (15). We used the relative green/ red fluorescence intensity ratios as a proxy measure to assess the integrity of the mycobacterial cell envelope. We observed that cells exposed to C_{60} or C_{90} had significantly decreased relative green/red fluorescence ratios with values of 0.634 and 0.608, respectively, when compared to control cells exposed only to the oleic acid:DMSO dispersant, suggesting a significant drop in the integrity of the cell envelope upon exposure to the CNMs.

We used ethidium bromide (EtBr) as a molecular probe to assess the effects of the CNMs on the transport processes across the mycobacterial cell wall. EtBr emits strong red fluorescence inside cells and weak fluorescence outside the cellular environment, making it a good tracer for studying accumulation and efflux processes in bacterial cells (30). We observed that fullertubes and fullerenes caused an increase in the accumulation of EtBr (Fig. 4 B-D). Specifically, C_{60} caused a 20 % increase, while C_{90} led to an increase of around 30 % in the measured endpoint EtBr fluorescence compared to the control (Fig. 4D). Additionally, we observed that the fullertubes and fullerenes did not significantly affect the efflux activity of *M. smegmatis* (Fig. 4F, Fig. 2S).

We used the molecular probe dichlorofluorescein (DCF) to investigate the molecular environment of *M. smegmatis* exposed to fullertubes and fullerenes. DCF is introduced into the cellular environment as dichlorofluorescein diacetate (DCFDA), which can cross the cellular membrane (31). Inside the cell, DCFDA is cleaved by intracellular esterases to

dichlorodihydrofluorescein ($DCFH_2$), which can then be oxidized to DCF by intracellular reactive oxygen species (ROS) and fluoresce green (31). We found that cells exposed to C_{60} and C_{90} had significantly decreased relative green fluorescence with (arbitrary) values of 0.519 and 0.484, respectively, compared to 1.0 for control cells (Fig. 4 E). Decreases in the relative green fluorescence of cells could indicate either a change in the redox state of the cell or a change in the integrity of the cell membrane. Taking the sum of all our data together, we interpret these decreases in the relative green fluorescence of cells exposed to C_{90} and C_{60} as primarily indicative of a loss in the integrity of the mycobacterial cell membrane.

3.4 Fullertubes and fullerenes disrupt biofilm formation in *Mycobacterium smegmatis.*

As fullertubes and fullerenes showed antimicrobial activity against *M. smegmatis* in our assays described above, we examined whether they could inhibit biofilm formation. We measured the effects of the fullertubes and fullerenes on floating (pellicle) biofilm formation at 72 h after exposure to fullerenes or fullertubes. In comparison to the Msm cells, the biofilm was inhibited by 20% in presence of 0.08% v/v solution of oleic acid:DMSO solvent control. This control group was established as the baseline at 100%, and the biofilm formation was calculated for 0.4 ug/mL C_{60} and C_{90}. At a concentration of 0.4 µg/mL, fullertubes inhibited biofilm formation by about 70% and fullerenes inhibited biofilm formation by 90%. At 0.2 µg/mL, fullertube and fullerenes treatment resulted in no appreciable inhibition of biofilm formation (Fig. 5A, Fig 5B). These findings suggest that fullertubes and fullerenes exhibit a concentration-dependent ability to inhibit the formation of mycobacterial biofilms.

3.5 Fullertubes and fullerenes do not show synergistic activity with isoniazid or cause *Mycobacterium smegmatis* to enter a dormant state.

We investigated the consequences of exposure to fullertubes or fullerenes on the activity of isoniazid which is known to interfere with mycobacterial cell wall synthesis (32). *M. smegmatis* cells were treated with fullertubes or fullerenes in combination with isoniazid for 24 h, alongside respective controls. The cultures were spread-plated on Middlebrook 7H10 agar plates and CFUs were determined. The CNMs significantly decreased cell viability on their own (Fig. 6). The addition of C_{90} or C_{60} along with isoniazid at 2 µg/mL or 10 µg/mL did not significantly affect the viability of the cell population when compared to the respective control containing only oleic acid:DMSO along with isoniazid. Thus, the CNMs did not show a synergistic effect with isoniazid at the two concentrations tested.

In order to investigate whether the CNMs induced *M. smegmatis* to enter a dormant state and therefore caused a decrease in CFU counts on agar plates, the serially-diluted cultures were also subjected to the MPN assay in parallel. As shown in Fig. 6, the MPN estimate for the controls exposed to oleic acid:DMSO were about 4-fold higher than the respective CFUs. The MPN estimate for cells exposed to C_{60} were about 3-fold higher than the CFUs and the MPN value for C_{90}-treated cells were nearly the same as the CFUs obtained. The viable cell count for the C_{60}-treated cells was 18% of the oleic acid:DMSO control by the CFU assay and 15% of this control by the MPN assay. For C_{90}-treated cells, the viable counts compared to the oleic acid:DMSO control were 18% by CFUs and 3% by MPN values. Since the viable cell counts in the CNM-treated samples by the MPN assay were similar or lower than the respective CFUs, we conclude that the exposure of the log-phase *M. smegmatis* cells to the CNMs led to loss of cell viability and did not cause the cells to enter dormancy.

4. Discussion

The antimicrobial activities of the recently isolated fullertubes have not been evaluated. Prior to this study, the effects of fullertubes and fullerenes had not been tested on *M. smegmatis* or *M. abscessus*. The antibacterial activity of C_{60} against both Gram-positive and Gram-negative strains of bacteria has been demonstrated earlier (10). C_{70}, a compound with a structure similar to C_{60}, has also been studied to a lesser extent. The study by Zhang et al. investigated the effects of functionalized C_{70} in the form of C_{70}-(ethylenediamine) on *E. coli* and *S. aureus*. They found that it can suppress the growth of drug-resistant strains of these organisms (11). The closest related compounds tested against mycobacteria are graphene oxide-linezolid nanoparticles, which possess anti-mycobacterial properties (33). However, the novel fullertubes have not been investigated for antimicrobial activities.

A major hindrance in utilizing pristine carbon nanomaterials in biological systems is their hydrophobic nature. The toxicity of fullerenes towards mammalian cells have been investigated in several studies over 25 years (34). Although fullerenes localized to cell membranes and caused oxidative damage to DNA, they did not show acute or sub-acute toxicity in rodents. Surprisingly, aqueous C_{60} suspension protected liver from ROS-mediated toxicity in rats and oral administration of fullerenes dissolved in olive oil doubled the life-span of rats (34). Some previous studies modified fullerenes using functional groups to make them more polar or by enveloping the fullerenes in aqueous suspensions of liposomes by heavy sonication or stirring (7). Other studies have prepared suspensions of fullerenes in water (8). Pristine nC_{60}, in fullerene water suspensions (FWS) have been shown to have antimicrobial activity against many gram-negative and gram-positive microorganisms, such as *E. coli* and *B. subtilis* (3, 10). CNMs, such as graphene oxide nanoparticles, have been shown to decrease the cell viability of *M. tuberculosis* (33, 35). We prepared dispersions of pristine fullertubes (nC_{90}) and fullerenes (nC_{60}) in an oleic acid:DMSO dispersant, which allowed the use of much smaller quantities of the fullertubes in our preparations. These dispersions showed anti-mycobacterial activities in the concentration range of 0.2 – 1.0 µg/mL against both *M. smegmatis* and *M. abscessus* suggesting a similar mode of action against mycobacteria (Fig. 1). C_{90} showed significant ($p<0.05$) anti-mycobacterial activity at the 0.2 µg/mL concentration. Our observed range of activity for both fullertubes and fullerenes falls in the general range of antimicrobial activity of previously reported C_{60} FWS (3, 10).

Previous studies of FWS have demonstrated that the particle size distribution of fullerene nanoparticle suspensions is related to their antibiotic activity (10). We characterized the particle size distributions for our C_{60} dispersion by dynamic light scattering. We found that our C_{60} dispersion showed only one major peak, with an average particle diameter of 416.5 ± 140.2 nm (Average± SD; Fig. S1). This suggested that our C_{60} dispersion was primarily monodispersed. Compared to studies of FWS, our C_{60} dispersion had a generally larger size. We attempted to control the particle size distribution of the C_{60} dispersion by sequentially filtering it through 0.45-micron and 0.2-micron nylon filters. We also attempted to measure the particle size distributions of the prepared C_{90} dispersion; however, we were unable to accurately determine a mean particle size as we suspect the dispersed particles were below the theoretical detection limit of 0.3 nm on the Zetasizer Nano ZS90. Furthermore, the C_{90} dispersion did not sediment over several months suggesting that the C_{90} was completely dissolved in the dispersant. Given that the particle sizes of the fullertube and fullerene dispersions are likely different, we are unable to make direct comparisons between the two.

Mycobacteria contain complex, multi-layered, lipid-rich cell walls that play a crucial role in mycobacterial pathogenesis, conferring key traits such as tolerance to antibiotics and the ability to form biofilms (2, 36-38). The interactions of fullerenes with biological membranes have been well-studied in other organisms. These findings suggest that fullerenes can aggregate in hydrophobic membranes, causing damage (3, 39, 40). This aggregation has primarily been attributed to the π-π stacking resulting from the highly conjugated electronic systems on the surface of fullerenes (39). The hydrophobic nature of the mycobacterial cell wall possibly predisposes it to fullertube and fullerene insertion and damage. Our scanning electron micrographs of *M. smegmatis* and *M. abscessus* exposed to fullertubes and fullerenes reveal that the bacilli were damaged after 24 h exposure (Fig. 2). Cellular debris was observed in many of the micrographic fields of the treated cells, suggesting that the fullertube and fullerene interactions with the mycobacterial cell wall resulted in physical damage and leakage of the cellular contents. Our observation of the loss of acid-fast staining property by *M. smegmatis* cells exposed to the fullertubes and fullerenes is suggestive of perturbation of the mycobacterial membrane and the mycolic acid layer in particular (Fig. 3).

We used fluorescent dyes as molecular probes in four different assays to quantitatively assess the damage to the mycobacterial cell wall and the resulting loss of integrity of the cells. The SYTO-9/ Propidium Iodide, membrane integrity assay has previously been used to describe the effects of various nanoparticles on bacterial membranes (15, 41). SYTO-9 can permeate all

cells, bind to DNA and fluoresce green whereas cells with damaged membranes favor the entry of PI (15, 41). The concurrent binding of SYTO-9 and PI results in the quenching of the SYTO-9 signal and a decrease in the green/red fluorescence ratio (Fig. S4-A) (15). We have used the green/red fluorescence ratio as a proxy for the integrity of the mycobacterial cellular envelope (Fig. 4 A). The significant decrease in the green/red fluorescence ratio of cells treated with C_{90} and C_{60} suggests an increased permeabilization of the mycobacterial cell envelope after exposure to these CNMs. In the EtBr transport assay, *M. smegmatis* cells treated with fullertubes and fullerenes showed increased EtBr accumulation compared to the dispersant control. However, the efflux of EtBr was not significantly affected (Fig. 4. B-D, F, Fig. S2). These observations suggest that the increased accumulation of EtBr could be due to the membrane damage caused by fullertubes and fullerenes rather than by the inhibition of efflux pumps (Fig. S4-B).

The third molecular probe that we used was dichlorofluorescein (DCF), which functions with a distinct mechanism from the other molecular probes used in this study. The dichlorofluorescein diacetate used in this assay is thought to permeate the cell envelope and is modified to dichlorofluorescein dihydride which is subsequently oxidized within the cell to form the green fluorescing dichlorofluorescein (Fig S4-B). This molecular probe traditionally measures reactive oxygen species (ROS), such as various intracellular peroxides and hydroxides. The use of this probe with fullerenes and other oxidizing nanoparticles has come under some controversy primarily due to how it has been observed to be oxidized directly by fullerenes, ultimately leading to a larger raw-fluorescence intensity. Additionally, previous studies have shown that the dichlorofluorescein assay is sensitive to the leakage of DCF and $DCFH_2$ out of the cell (31). A previous study reported higher green fluorescence due to interference by fullerene water suspensions (42). In order to avoid the direct extracellular oxidation of dichlorofluorescein dihydride ($DCFH_2$) by fullertubes and fullerenes, we added a wash step where the growth medium containing the fullertubes and fullerenes was removed before exposure of the washed cells to the molecular probe. When the wash step was included, we observed that cells treated with C_{60} or C_{90} displayed a significantly decreased normalized green fluorescence intensity compared to the oleic acid:DMSO control (Fig. 4F). This observation suggests that C_{60} and C_{90} are either increasing the efflux of DCF or increasing the permeability of the mycobacterial cell envelope to polar compounds such as DCF and $DCFH_2$, or are acting as scavengers of intracellular ROS (31, 43). In light of our findings that suggest

that fullertubes and fullerenes do not affect the efflux activities of *M. smegmatis* (Fig. 4F, Fig. S2), the latter two explanations are more likely.

The FOX II lipid peroxidation assay (Fig. S3) functions under the principle that the Xylenol Orange and Ferrous components of the assay are selectively oxidized by lipid peroxides (44). To address the previously noted interference that fullertubes and fullerenes have in the efficacy of the FOX II assay, we included a similar wash step to the one used in the DCF assay (42). Our observations revealed that fullertubes and fullerenes did not induce increased production of ROS nor did we observe any lipid peroxidation. However, the positive control using 50 mM H_2O_2 validated the FOX assay by demonstrating lipid peroxidation. These findings suggest that ROS may not be directly responsible for the antibacterial activity of fullerenes and fullertube prepared as dispersions in oleic acid:DMSO in this study. These findings are consistent with studies of the effects of fullerene water suspensions on lipid peroxidation (42). Taken together, our observations from the assays with the fluorescent dyes suggest that fullertubes and fullerenes cause damage and increase the permeability of the mycobacterial cell wall.

There are few reports on the effects of carbon nanomaterials on bacterial biofilm formation (45). The effects of fullertubes on biofilm formation in any microorganism has not been investigated. We observed that fullertubes exhibited a significantly higher ($p<0.001$) inhibition of biofilm formation at a concentration of 0.4 µg/mL compared to the control. At this concentration, fullertubes and fullerenes reduced biofilm formation by 75 - 90 %. No appreciable loss in biofilm formation was noted at the 0.2 µg/mL concentration (Fig. 5).

Antibiotic resistance is another mycobacterial phenotype closely tied to the functionality of the cell envelope (46). The frontline antibiotic isoniazid inhibits mycolic acid synthesis, which is required for cell wall synthesis and is critical for the survival of the multiplying mycobacterial cell (32). Since we observed the deleterious effects of fullertubes and fullerenes on the mycobacterial cell wall and its acid-fast staining property that relies on staining of mycolic acids in the cell wall, we were interested in the potential consequences on isoniazid tolerance by the mycobacteria. The combination of C_{60} and isoniazid did not show any synergistic effects (Fig. 6). Since mycobacteria that enter a dormant state fail to show colony formation on agar plates but show viability by the MPN assay as described by others earlier (22, 23), we used the MPN assay to investigate whether the CNMs caused a decrease in CFUs on our agar plates by potentially inducing *M. smegmatis* to enter a dormant state. As expected, the MPN/mL estimates were higher than the actual CFUs/mL for *M. smegmatis* controls exposed to oleic

514 acid:DMSO. However, the MPN estimates indicated that only 3 % and 15 % of the cells
515 remained viable after exposure to C_{90} and C_{60} respectively. These values were similar or lower
516 than the respective cell viabilities determined by the CFU method. These results indicate that
517 the CNMs indeed killed the *M. smegmatis* cells instead of merely inducing them to enter a
518 dormant state. Since the C_{90} fullertubes are not commercially available, we were unable to test
519 the effects of fullertubes at higher concentrations or investigate their toxicity on mammalian
520 cells. In summary, we show that fullertubes and fullerenes inhibit mycobacterial cell growth by
521 damaging the cell wall and prevent biofilm formation in *M. smegmatis*.

ACKNOWLEDGEMENTS

The authors acknowledge Ryan Koenig for initiating this project. We also are grateful for help received from Dr. Dong Chen, Director of The Argast Family Imaging and Analysis Laboratories, Purdue University Fort Wayne, Dr. Benjamin Dattilo, Department of Biological Sciences and Dr. Liliya Frolova, Department of Chemistry, Purdue University Fort Wayne in the preparation of SEM samples. We express our gratitude to Mr. Jonathan Hall for the technical help received for acquiring the scanning electron microscopy (SEM) images. The support of the Department of Biological Sciences, Purdue University Fort Wayne in providing the infrastructure for the research is gratefully acknowledged.

FUNDING

VS received research funds from the Purdue University Fort Wayne Honors Research Grant. RG was supported by a Teaching Assistantship from the Department of Biological Sciences, Purdue University Fort Wayne. S.S. thanks the National Science Foundation for RUI Grant CHE-1856461 for financial support. SS and JD received funding from the Collaborative Research Grant, Purdue Fort Wayne Office of Sponsored Programs.

References

1. Stephanie F, Saragih M, Tambunan USF. Recent Progress and Challenges for Drug-Resistant Tuberculosis Treatment. Pharmaceutics. 2021;13(5).
2. Johansen MD, Herrmann JL, Kremer L. Non-tuberculous mycobacteria and the rise of Mycobacterium abscessus. Nat Rev Microbiol. 2020;18(7):392-407.
3. Lyon DY, Fortner JD, Sayes CM, Colvin VL, Hughe JB. Bacterial cell association and antimicrobial activity of a C60 water suspension. Environ Toxicol Chem. 2005;24(11):2757-62.
4. Xin Q, Shah H, Nawaz A, Xie W, Akram MZ, Batool A, et al. Antibacterial Carbon-Based Nanomaterials. Adv Mater. 2019;31(45):e1804838.
5. Al-Jumaili A, Alancherry S, Bazaka K, Jacob MV. Review on the Antimicrobial Properties of Carbon Nanostructures. Materials (Basel). 2017;10(9).
6. Raul PK, Thakuria A, Das B, Devi RR, Tiwari G, Yellappa C, et al. Carbon Nanostructures As Antibacterials and Active Food-Packaging Materials: A Review. ACS Omega. 2022;7(14):11555-9.
7. Bolshakova O, Lebedev V, Mikhailova E, Zherebyateva O, Aznabaeva L, Burdakov V, et al. Fullerenes on a Nanodiamond Platform Demonstrate Antibacterial Activity with Low Cytotoxicity. Pharmaceutics. 2023;15(7).
8. Koenig RM, Tian HR, Seeler TL, Tepper KR, Franklin HM, Chen ZC, et al. Fullertubes: Cylindrical Carbon with Half-Fullerene End-Caps and Tubular Graphene Belts, Their Chemical Enrichment, Crystallography of Pristine C(90)-D(5h)(1) and C(100)-D(5d)(1) Fullertubes, and Isolation of C(108), C(120), C(132), and C(156) Cages of Unknown Structures. J Am Chem Soc. 2020;142(36):15614-23.
9. Stevenson S, Liu X, Sublett DM, Jr., Koenig RM, Seeler TL, Tepper KR, et al. Semiconducting and Metallic [5,5] Fullertube Nanowires: Characterization of Pristine D(5h)(1)-C(90) and D(5d)(1)-C(100). J Am Chem Soc. 2021;143(12):4593-9.
10. Lyon DY, Adams LK, Falkner JC, Alvarez PJ. Antibacterial activity of fullerene water suspensions: effects of preparation method and particle size. Environ Sci Technol. 2006;40(14):4360-6.
11. Zhang J, Xu J, Ma H, Bai H, Liu L, Shu C, et al. Designing an Amino-Fullerene Derivative C(70)-(EDA)(8) to Fight Superbacteria. ACS Appl Mater Interfaces. 2019;11(16):14597-607.
12. Vijay S, Mukkayyan N, Ajitkumar P. Highly Deviated Asymmetric Division in Very Low Proportion of Mycobacterial Mid-log Phase Cells. Open Microbiol J. 2014;8:40-50.
13. Shehadat SA, Gorduysus MO, Hamid SSA, Abdullah NA, Samsudin AR, Ahmad A. Optimization of scanning electron microscope technique for amniotic membrane investigation: A preliminary study. Eur J Dent. 2018;12(4):574-8.
14. Inoue T, Osatake H. A new drying method of biological specimens for scanning electron microscopy: the t-butyl alcohol freeze-drying method. Arch Histol Cytol. 1988;51(1):53-9.
15. Horst AM, Vukanti R, Priester JH, Holden PA. An assessment of fluorescence- and absorbance-based assays to study metal-oxide nanoparticle ROS production and effects on bacterial membranes. Small. 2013;9(9-10):1753-64.
16. Paixao L, Rodrigues L, Couto I, Martins M, Fernandes P, de Carvalho CC, et al. Fluorometric determination of ethidium bromide efflux kinetics in Escherichia coli. J Biol Eng. 2009;3:18.
17. Vianna JS, Machado D, Ramis IB, Silva FP, Bierhals DV, Abril MA, et al. The Contribution of Efflux Pumps in *Mycobacterium abscessus* Complex Resistance to Clarithromycin. Antibiotics (Basel). 2019;8(3):153.
18. Thakur N, Sharma AN, Hade MD, Chhaya A, Kumar A, Jolly RS, et al. New Insights Into the Function of Flavohemoglobin in Mycobacterium tuberculosis: Role as a NADPH-Dependent Disulfide Reductase and D-Lactate-Dependent Mycothione Reductase. Front Cell Infect Microbiol. 2021;11:796727.

19. Patel YS, Mistry N, Mehra S. Repurposing artemisinin as an anti-mycobacterial agent in synergy with rifampicin. Tuberculosis (Edinb). 2019;115:146-53.
20. Recht J, Martinez A, Torello S, Kolter R. Genetic analysis of sliding motility in Mycobacterium smegmatis. J Bacteriol. 2000;182(15):4348-51.
21. Billman-Jacobe H, Sloan J, Coppel RL. Analysis of isoniazid-resistant transposon mutants of Mycobacterium smegmatis. FEMS Microbiol Lett. 1996;144(1):47-52.
22. Mukamolova GV, Turapov O, Malkin J, Woltmann G, Barer MR. Resuscitation-promoting factors reveal an occult population of tubercle Bacilli in Sputum. Am J Respir Crit Care Med. 2010;181(2):174-80.
23. Salina EG, Grigorov AS, Bychenko OS, Skvortsova YV, Mamedov IZ, Azhikina TL, et al. Resuscitation of Dormant "Non-culturable" Mycobacterium tuberculosis Is Characterized by Immediate Transcriptional Burst. Front Cell Infect Microbiol. 2019;9:272.
24. Blodgett R. Most Probable Number Determination from Serial Dilutions. FDA Bacteriological Analytical Manual Online, Appendix 2. 2006.
25. Blodgett RJ, Moruzzi G. The expanded application of most probable number to the quantitative evaluation of extremely low microbial count. PDA J Pharm Sci Technol. 2006;60(6):335-6.
26. Lelovic N, Mitachi K, Yang J, Lemieux MR, Ji Y, Kurosu M. Application of Mycobacterium smegmatis as a surrogate to evaluate drug leads against Mycobacterium tuberculosis. J Antibiot (Tokyo). 2020;73(11):780-9.
27. Sundarsingh T, Ranjitha J, Rajan A, Shankar V. Features of the biochemistry of Mycobacterium smegmatis, as a possible model for Mycobacterium tuberculosis. J Infect Public Health. 2020;13(9):1255-64.
28. Clary G, Sasindran SJ, Nesbitt N, Mason L, Cole S, Azad A, et al. Mycobacterium abscessus Smooth and Rough Morphotypes Form Antimicrobial-Tolerant Biofilm Phenotypes but Are Killed by Acetic Acid. Antimicrob Agents Chemother. 2018;62(3).
29. Yang S, Zhang F, Kang J, Zhang W, Deng G, Xin Y, et al. Mycobacterium tuberculosis Rv1096 protein: gene cloning, protein expression, and peptidoglycan deacetylase activity. BMC Microbiol. 2014;14:174.
30. Rodrigues L, Ramos J, Couto I, Amaral L, Viveiros M. Ethidium bromide transport across Mycobacterium smegmatis cell-wall: correlation with antibiotic resistance. BMC Microbiol. 2011;11:35.
31. Jakubowski W, Bartosz G. Estimation of oxidative stress in Saccharomyces cerevisae with fluorescent probes. Int J Biochem Cell Biol. 1997;29(11):1297-301.
32. Timmins GS, Deretic V. Mechanisms of action of isoniazid. Mol Microbiol. 2006;62(5):1220-7.
33. De Maio F, Palmieri V, Santarelli G, Perini G, Salustri A, Palucci I, et al. Graphene Oxide-Linezolid Combination as Potential New Anti-Tuberculosis Treatment. Nanomaterials (Basel). 2020;10(8).
34. Goodarzi G, Da Ros T, Conde J, Sefat F, Mozafari M. Fullerene: biomedical engineers get to revisit an old friend. Materials Today. 2017;20(8):460-80.
35. De Maio F, Palmieri V, De Spirito M, Delogu G, Papi M. Carbon nanomaterials: a new way against tuberculosis. Expert Rev Med Devices. 2019;16(10):863-75.
36. Chen H, Nyantakyi SA, Li M, Gopal P, Aziz DB, Yang T, et al. The Mycobacterial Membrane: A Novel Target Space for Anti-tubercular Drugs. Front Microbiol. 2018;9:1627.
37. Daffé M, Quémard A, Marrakchi H. Mycolic Acids: From Chemistry to Biology. In: Geiger O, editor. Biogenesis of Fatty Acids, Lipids and Membranes. Cham: Springer International Publishing; 2017. p. 1-36.
38. Esteban J, Garcia-Coca M. Mycobacterium Biofilms. Front Microbiol. 2017;8:2651.
39. Ren L, Jing Z, Xia F, Zhang JZ, Li Y. Toxic Effect of Fullerene and Its Derivatives upon the Transmembrane beta(2)-Adrenergic Receptors. Molecules. 2022;27(14).

40. Santos SM, Dinis AM, Peixoto F, Ferreira L, Jurado AS, Videira RA. Interaction of fullerene nanoparticles with biomembranes: from the partition in lipid membranes to effects on mitochondrial bioenergetics. Toxicol Sci. 2014;138(1):117-29.
41. Lyon DY, Alvarez PJJ. Fullerene Water Suspension (nC60) Exerts Antibacterial Effects via ROS-Independent Protein Oxidation. Environmental Science & Technology. 2008;42(21):8127-32.
42. Lyon DY, Brunet L, Hinkal GW, Wiesner MR, Alvarez PJ. Antibacterial activity of fullerene water suspensions (nC60) is not due to ROS-mediated damage. Nano Lett. 2008;8(5):1539-43.
43. Ma H, Zhao J, Meng H, Hu D, Zhou Y, Zhang X, et al. Carnosine-Modified Fullerene as a Highly Enhanced ROS Scavenger for Mitigating Acute Oxidative Stress. ACS Applied Materials & Interfaces. 2020;12(14):16104-13.
44. Pinto Mdel C, Tejeda A, Duque AL, Macias P. Determination of lipoxygenase activity in plant extracts using a modified ferrous oxidation-xylenol orange assay. J Agric Food Chem. 2007;55(15):5956-9.
45. Cui F, Li T, Wang D, Yi S, Li J, Li X. Recent advances in carbon-based nanomaterials for combating bacterial biofilm-associated infections. J Hazard Mater. 2022;431:128597.
46. Jarlier V, Nikaido H. Mycobacterial cell wall: structure and role in natural resistance to antibiotics. FEMS Microbiol Lett. 1994;123(1-2):11-8.

FIGURE LEGENDS

Figure 1. Dispersions of fullerenes (C_{60}) and fullertubes (C_{90}) show antimicrobial activity against *M. smegmatis* and *M. abscessus*. *M. smegmatis* cells in log-phase (10^4 CFUs/mL) were exposed for 40 h with shaking at 37 °C to C_{60} or C_{90} as dispersions in oleic acid:dimethyl sulfoxide (DMSO; 1:3, v/v) at final concentrations of 0.2 µg/mL or 1 µg/mL in culture medium. **A,** Colony forming units (CFUs/mL) from duplicates of a representative experiment are shown as average ± SD. **B,** Viability of *M. smegmatis* cells exposed to C_{60} or C_{90} is shown as a percent of control cells exposed to oleic acid:DMSO. Percent survival values (average ± SD) from three independent experiments. **C,** CFUs/mL of *M. abscessus* cells exposed for 205 h to C_{60} or C_{90} at a concentration of 1 µg/mL. **D,** Percent survival of *M. abscessus* compared to oleic acid:DMSO control. One-way ANOVA and Tukey's HSD post hoc test were performed to determine significance. *p<0.05; ****p<0.0001.

Figure 2. Exposure of *M. smegmatis* and *M. abscessus* to C_{60} or C_{90} induces changes in cell morphology. Scanning electron micrographs of untreated cells, cells exposed to 1:3 oleic acid:DMSO (0.1 %, v/v) and cells exposed to dispersions of C_{60} and C_{90} at 0.2 µg/mL. *M. smegmatis* cells were observed after 2 h and 24 h and *M. abscessus* cells were observed after 24 h of exposure. The cells were collected over a 0.22-micron polycarbonate filter, dried, and sputter coated with a gold coating at a thickness of 2 nm. The cells were imaged at a voltage of 3.00 kV and a magnification of 15,000X. Representative fields are shown for each treatment.

Figure 3. Exposure of *M. smegmatis* to C_{60} or C_{90} induces changes in acid-fast staining morphology. *M. smegmatis* cells in log-phase (10^4 CFUs/mL) were exposed for 40 h with shaking at 37 °C to C_{60} or C_{90} as dispersions in oleic acid:dimethyl sulfoxide (DMSO; 1:3, v/v) at final concentrations of 0.2 µg/mL in culture. The cells were collected and stained with carbolfuchsin for acid-fast staining. The cells were viewed and photographed under brightfield at 1000X. Representative fields for each group across three independent experiments are depicted.

Figure 4. *M. smegmatis* cell envelope integrity is compromised, and permeability is increased by exposure to C_{60} or C_{90}. A, The relative green (Ex. 485 nm/ Em. 528 nm)/ red (Ex. 530 nm/ Em. 590 nm) fluorescence ratios of *M. smegmatis* cells treated with C_{60} or C_{90} or control cells exposed only to oleic acid:DMSO (1:3, v/v). Cells were washed after exposure to CNMs and then stained with a 2X SYTO-9/ propidium iodide solution. Treated cells were exposed to C_{60} or C_{90} (0.2 µg/mL) for 2 hours. The ratios were calculated against the *M. smegmatis* + oleic acid:DMSO control and normalized using CFUs obtained from agar plating.

The kinetics of EtBr accumulation in the presence of 0.4 µg/mL C_{60} **(B)** and C_{90} **(C)** compared to verapamil (VP, 75 µg/mL) and oleic acid:DMSO controls are shown. A representative experiment from three independent repeats is depicted. **D,** The normalized fluorescence at the 60 min endpoint after EtBr accumulation in the presence of 0.4 µg/mL C_{60} or C_{90}. **E,** The relative green fluorescence (Ex. 485 nm/ Em. 528 nm) of *M. smegmatis* cells treated with C_{60} or C_{90} (0.2 µg/mL) for 2 hours and exposed to dichlorodihydrofluorescein diacetate. The relative green fluorescence ratios are calculated against the *M. smegmatis* + oleic acid:DMSO control and normalized using CFUs obtained from agar plating. Average ± SD over three independently performed experiments are depicted. **F,** The normalized fluorescence at the 60 min endpoint after EtBr efflux in the presence of 0.4 ug/mL C_{60} or C_{90}. Statistical significance calculated by one-way ANOVA with a post-hoc Tukey test. *p<0.05, **p < 0.01, ***p < 0.001.

Figure 5. Fullerenes and fullertubes inhibit pellicle biofilm formation in *M. smegmatis*. Cells exposed to fullertubes and fullerenes were allowed to form biofilms under static conditions at 37 °C for 72 h in glass tubes. Biofilm formation was then quantified by staining with Crystal Violet and measuring absorbance at 600 nm. **A**, Floating biofilm formation after three days in the presence of 0.2 and 0.4 µg/mL of C_{60} and C_{90} concentrations. **B**, Quantitation of biofilm formation in the presence of fullertubes and fullerenes compared to controls exposed to oleic acid:DMSO. Average ± SD from three independent experiments are depicted. Statistical significance was determined by one-way ANOVA with Tukey's post hoc test. *p<0.05; ****p<0.0001.

Figure 6. Fullertubes and fullerenes do not induce dormancy in *M. smegmatis* or show synergistic action with isoniazid. *M. smegmatis* (Msm) cells were exposed to C_{90} or C_{60} (0.2 µg/mL) for 2 h at 37 °C, and then exposed to isoniazid at a final concentration of 2 µg/mL or 10 µg/mL for an additional 24 h at 37 °C. Appropriate serial dilutions were spread-plated onto Middlebrook 7H10 agar plates or assayed for Most Probable Numbers (MPN). Three independent repeats performed. Data shown as average ± SD for CFUs/mL. MPN index values per mL from a representative experiment shown. The 95% confidence limits (lower, upper) were as follows: Msm + Oleic:DMSO, (3.7, 42); Msm + C_{60}, (0.46, 9.4); Msm + C_{90}, (0.09, 1.8). Statistical significance was determined by one-way ANOVA with Tukey's post hoc test. ***, p<0.001.

SUPPLEMENTARY FIGURE LEGENDS

Figure S1. Particle sizes in the C_{60} stock dispersion. The prepared 1 mg/mL C_{60} dispersion was diluted 1:100 in 1:3 oleic acid:DMSO. The particle size distributions were measured by dynamic light scattering (DLS) in a Zetasizer Nano. Particle size percent intensities within the range of 1-1000 nm shown. The average particle diameter was determined across three independent measurements.

Figure S2. Fullertubes and fullerenes do not affect the efflux activity of EtBr in *M. smegmatis*. *M. smegmatis* cells were loaded with EtBr at 3 µg/mL in the presence of VP at half its MIC and the assay was carried out at 37°C. Efflux of EtBr is inhibited by Verapamil (VP) but not by C_{60} **(A)** or by 0.4 µg/mL C_{90} **(B)**.

Figure S3. Fullertubes and fullerenes do not generate lipid peroxides in *M. smegmatis*. Cells at 10^6 CFUs/mL in PBST were exposed to varying concentrations (0.2 and 0.4 µg/mL) of C_{60} and C_{90} for 4 h at 37°C. Cells treated only with oleic acid: DMSO (1:3, v/v) served as the control for normalization of absorbance readings. Cells treated with 50 mM H_2O_2 served as the positive control. The data show the average ± standard deviation across three independent experiments. One-way ANOVA and Tukey's post hoc test were performed to determine significance. *$p < 0.05$, H_2O_2: Hydrogen peroxide.

Figure S4. Hypothetical molecular mechanisms for the SYTO-9/Propidium Iodide and dichlorofluorescein molecular probes. A, The SYTO-9/Propidium Iodide (PI) molecular probes can evaluate the integrity of the cellular membrane. SYTO-9, permeates all cellular membranes, binds to intracellular DNA and fluoresces green. PI preferentially enters cells with damaged membranes, binds intracellular DNA and fluoresces red. Fluorescence quenching between the two probes skews the green/red fluorescence ratio. A decreased green/red fluorescence ratio indicates compromised membrane integrity (15). **B,** In the Dichlorofluorescein (DCF) redox assay, the cell is exposed to the probe as dichlorofluorescein diacetate (DCFDA), which can cross the cell membrane. DCFDA is then cleaved to dichlorofluorescein dihydride ($DCFH_2$) by intracellular esterases and then oxidized to the green fluorescing DCF. Under conditions of decreased membrane integrity, these compounds may leak out of the cell, reducing the measured fluorescence (15, 31).

Data Availability Statement

All data associated with this manuscript are presented as figures or supplemental figures and are included in this manuscript.

758 FIGURE 1

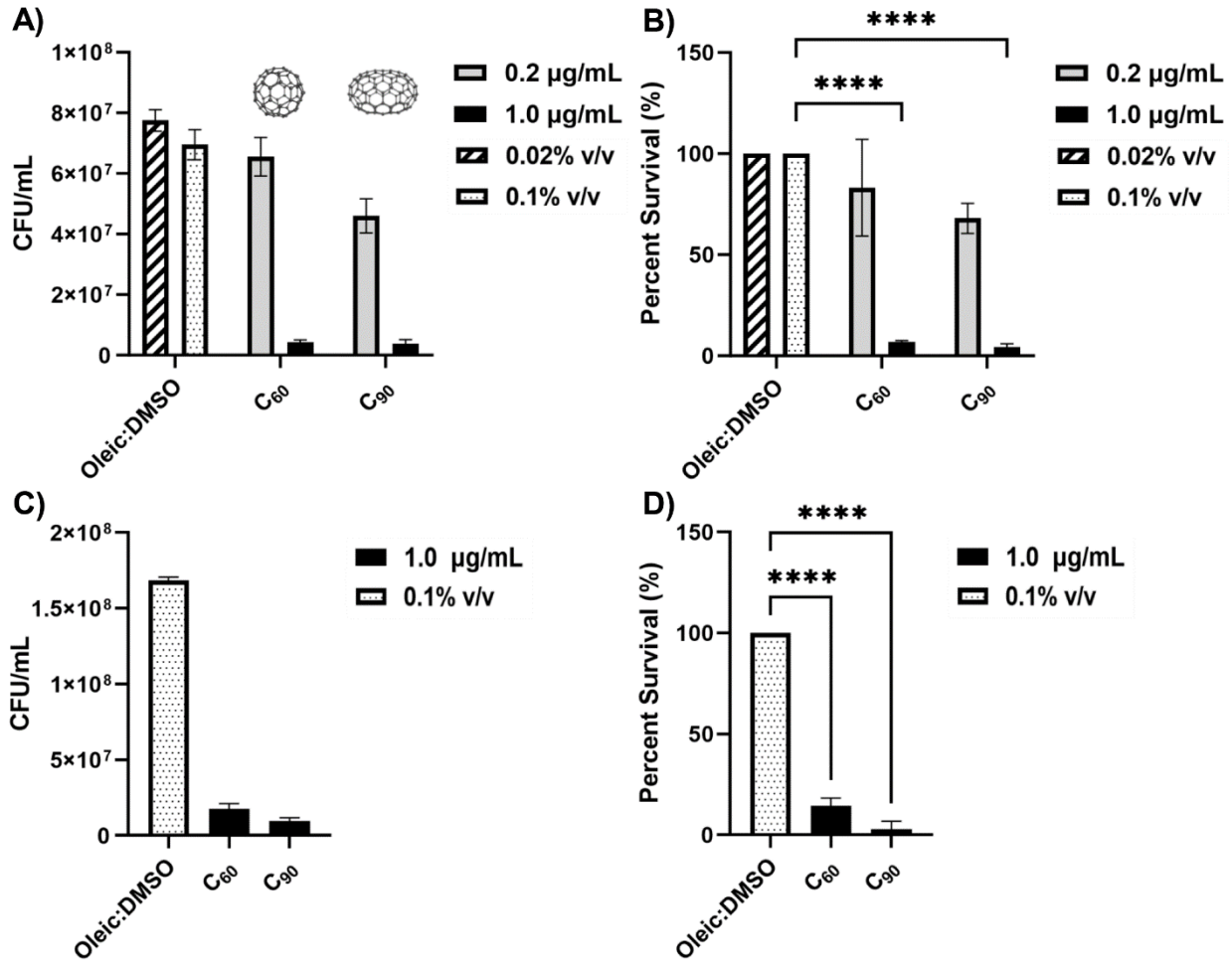

759

760

761 FIGURE 2

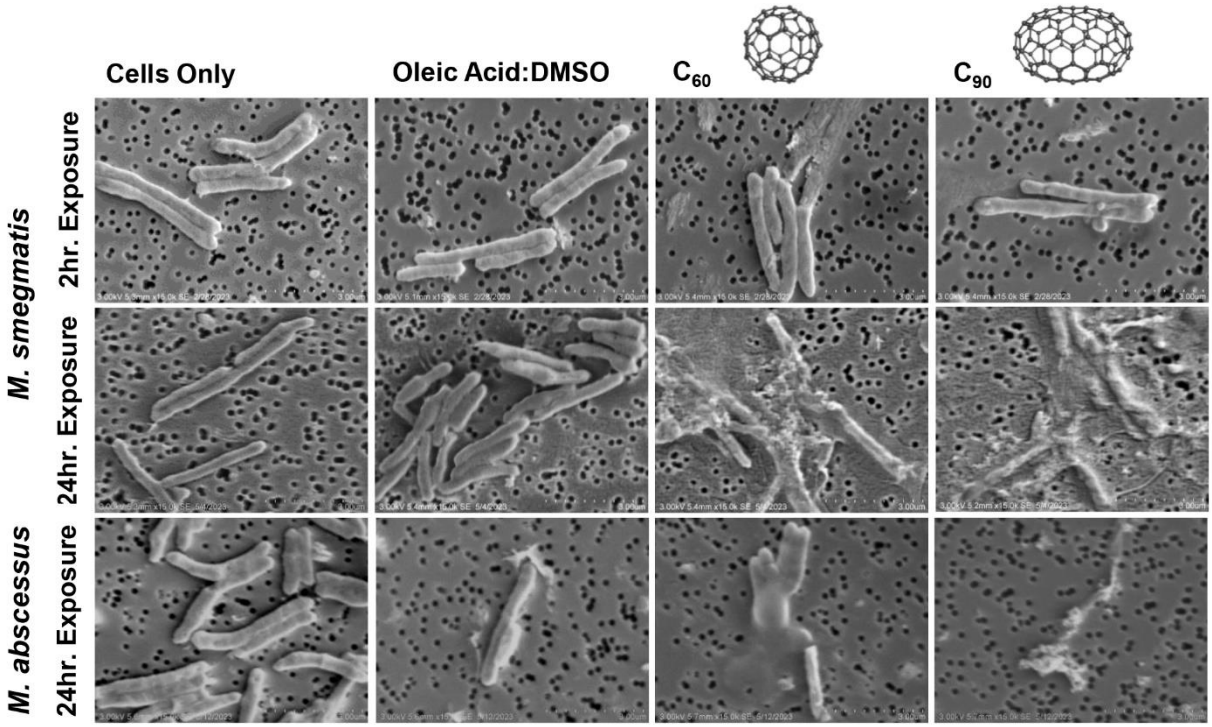

762

763

764 FIGURE 3

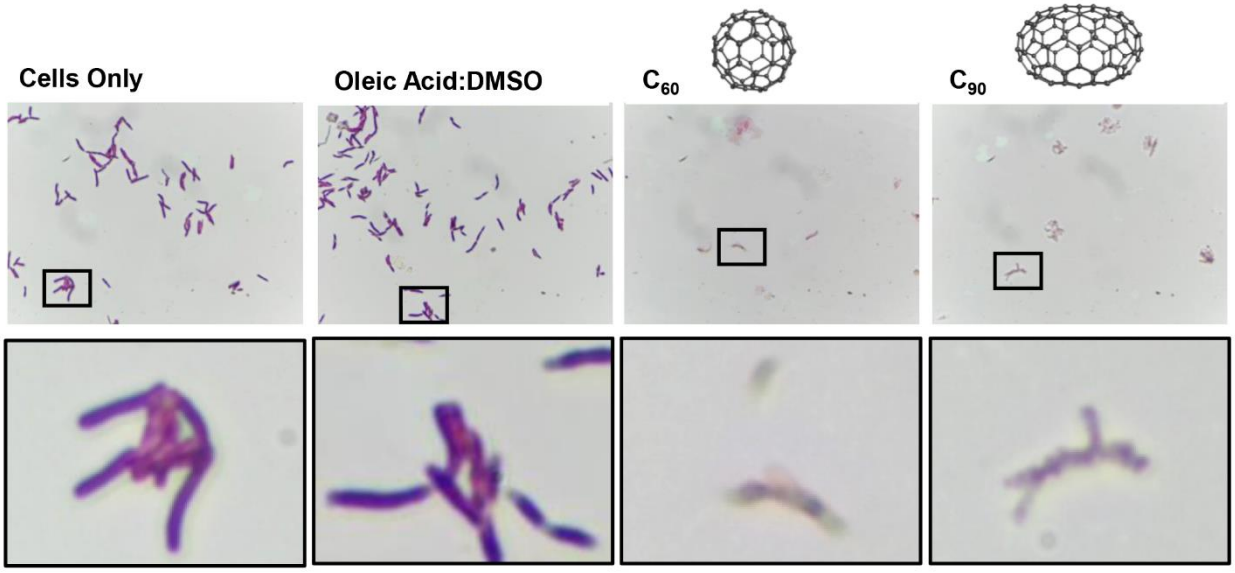

765

766

FIGURE 4

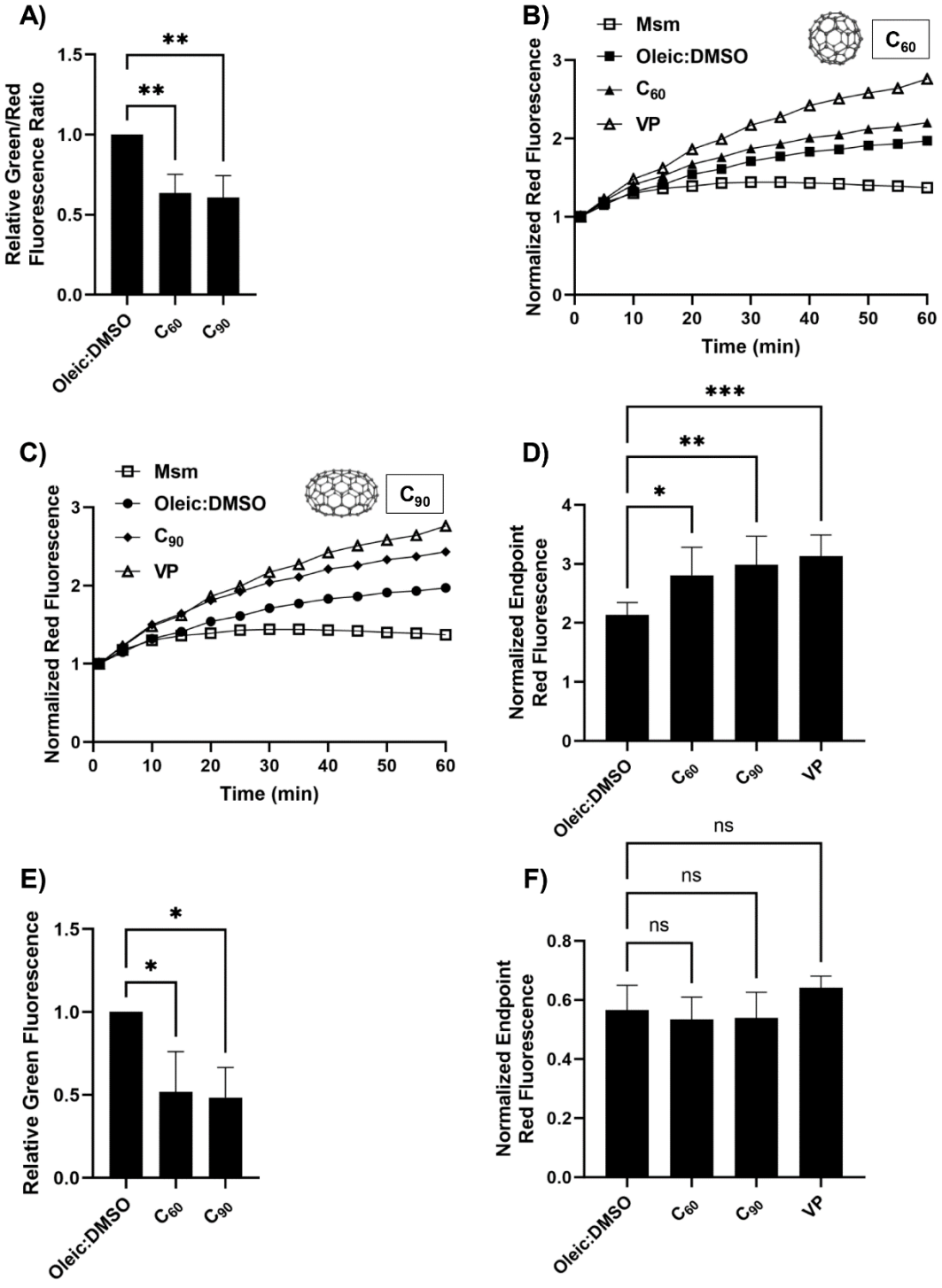
A)
Relative Green/Red Fluorescence Ratio
1.5
1.0
0.5
0.0
**
**
Oleic:DMSO
C60
C90
B)
Msm
Oleic:DMSO
C60
VP
C60
Normalized Red Fluorescence
3
2
1
0
0
10
20
30
40
50
60
Time (min)
C)
Msm
Oleic:DMSO
C90
VP
C90
Normalized Red Fluorescence
3
2
1
0
0
10
20
30
40
50
60
Time (min)
D)
***
**
*
Normalized Endpoint Red Fluorescence
4
3
2
1
0
Oleic:DMSO
C60
C90
VP
E)
Relative Green Fluorescence
1.5
1.0
0.5
0.0
*
*
Oleic:DMSO
C60
C90
F)
ns
ns
ns
Normalized Endpoint Red Fluorescence
0.8
0.6
0.4
0.2
0.0
Oleic:DMSO
C60
C90
VP

771 FIGURE 5

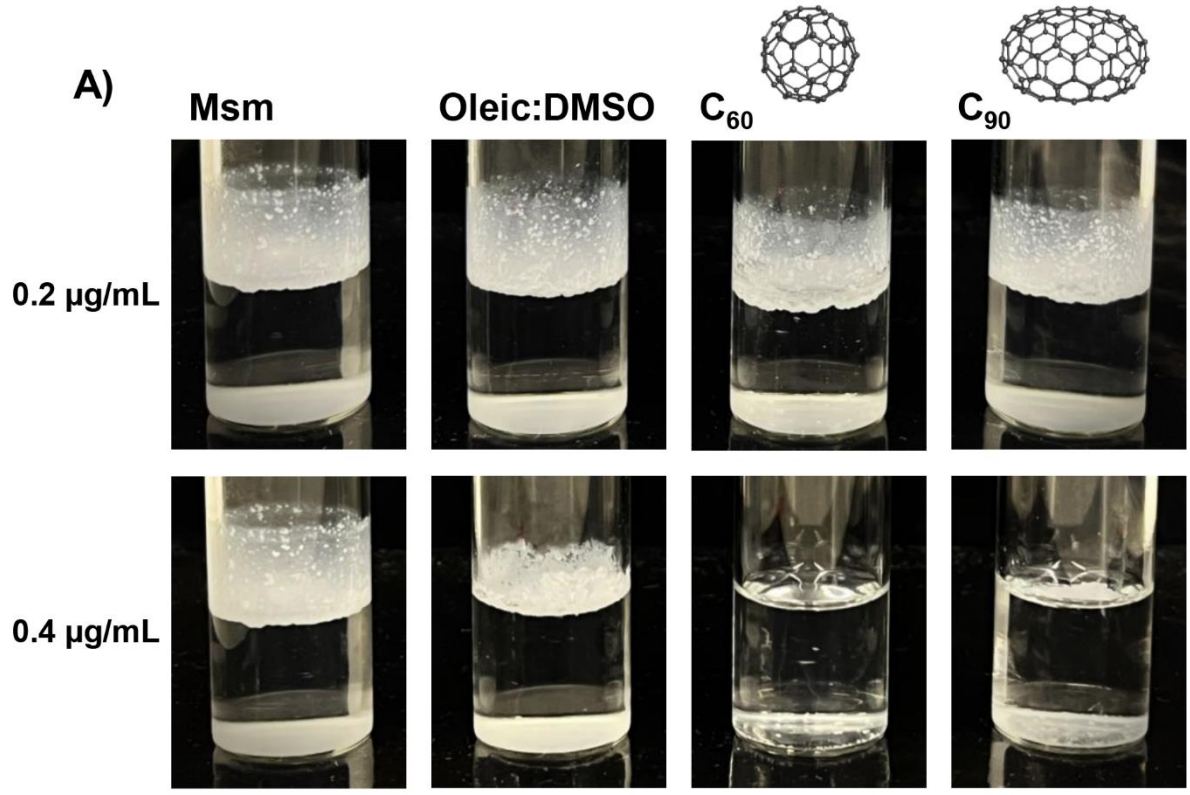

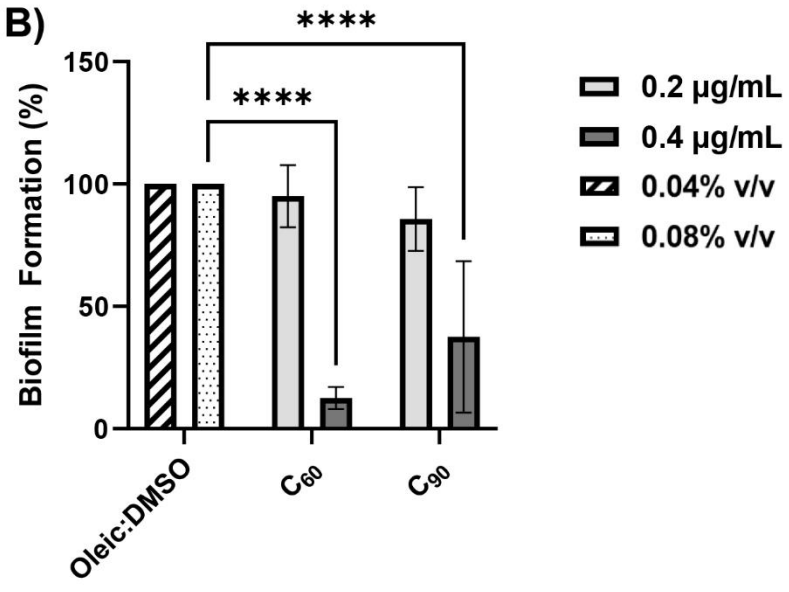

772

773

774

775 FIGURE 6

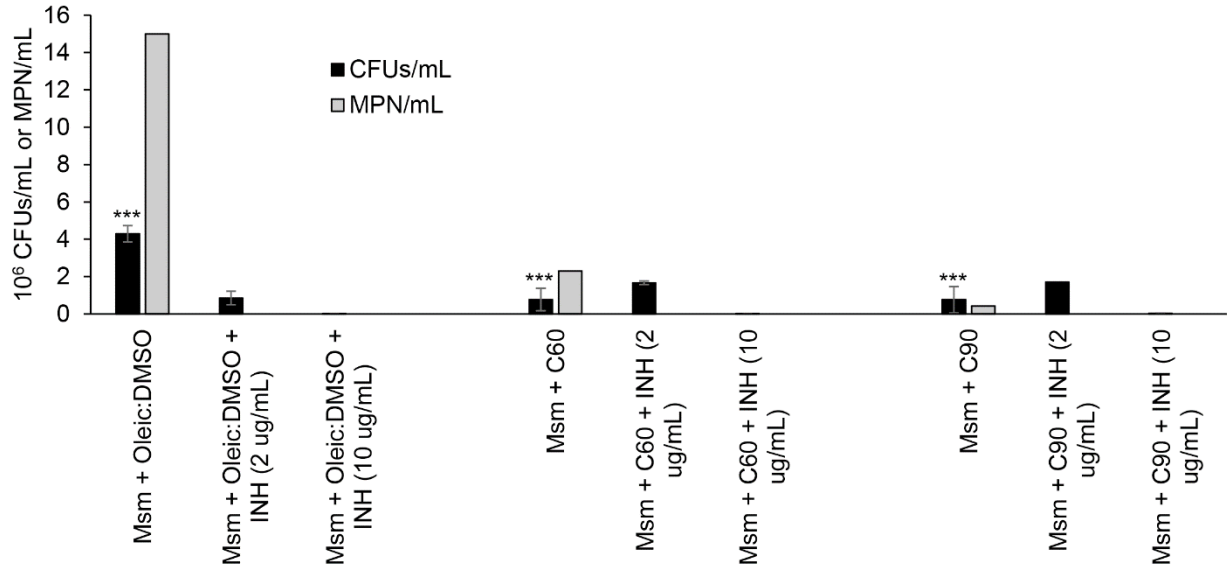

776

777

778 FIGURE S1

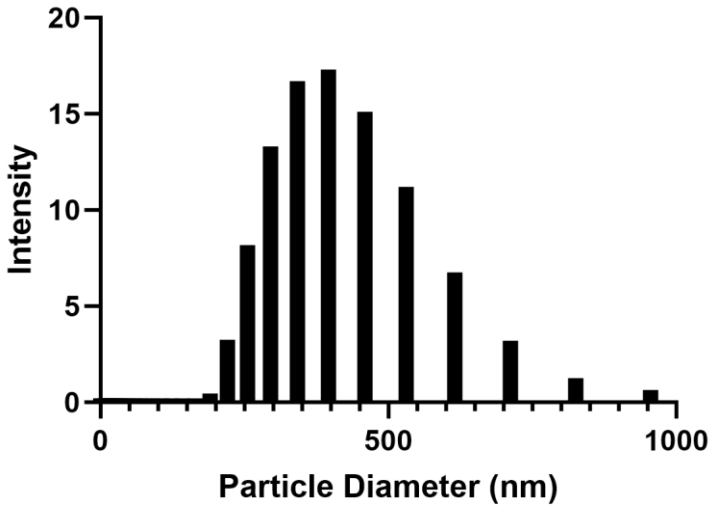

779

780

781 FIGURE S2

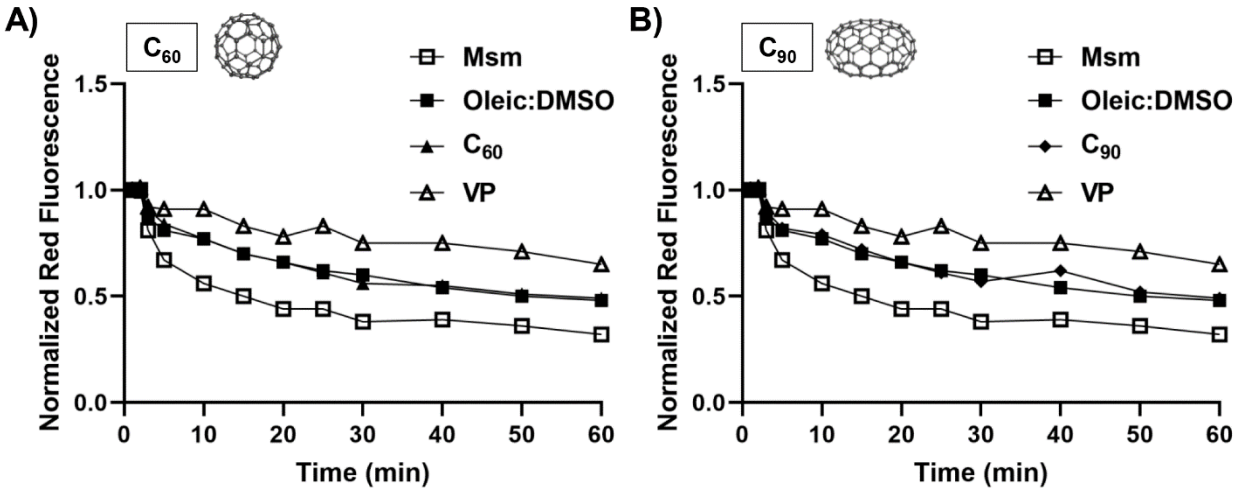

782

783

784 FIGURE S3

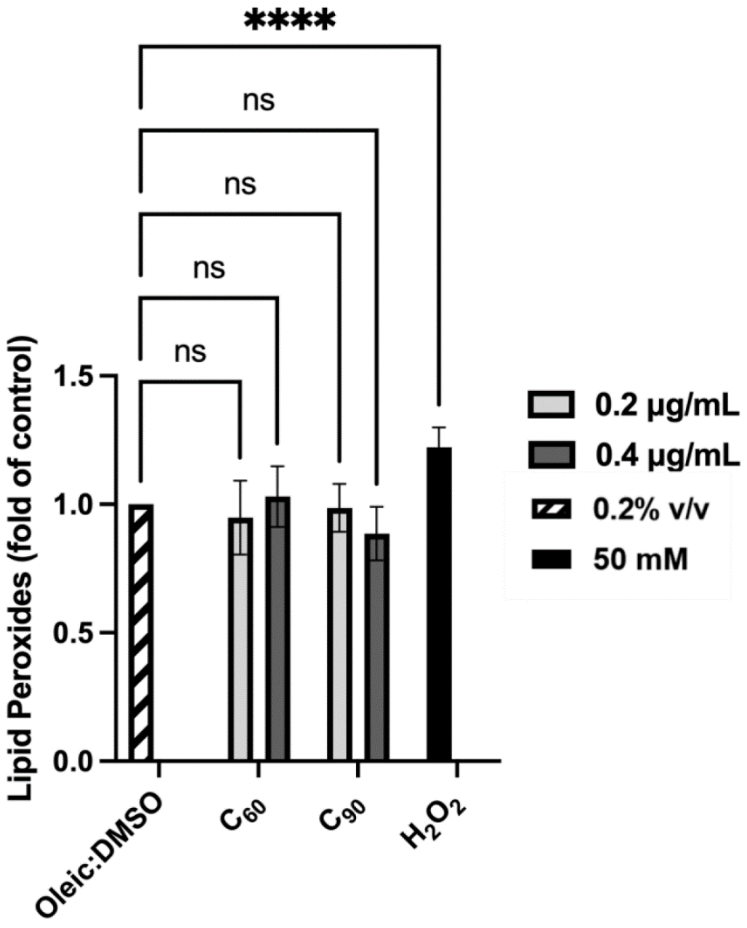

785

786

787 FIGURE S4

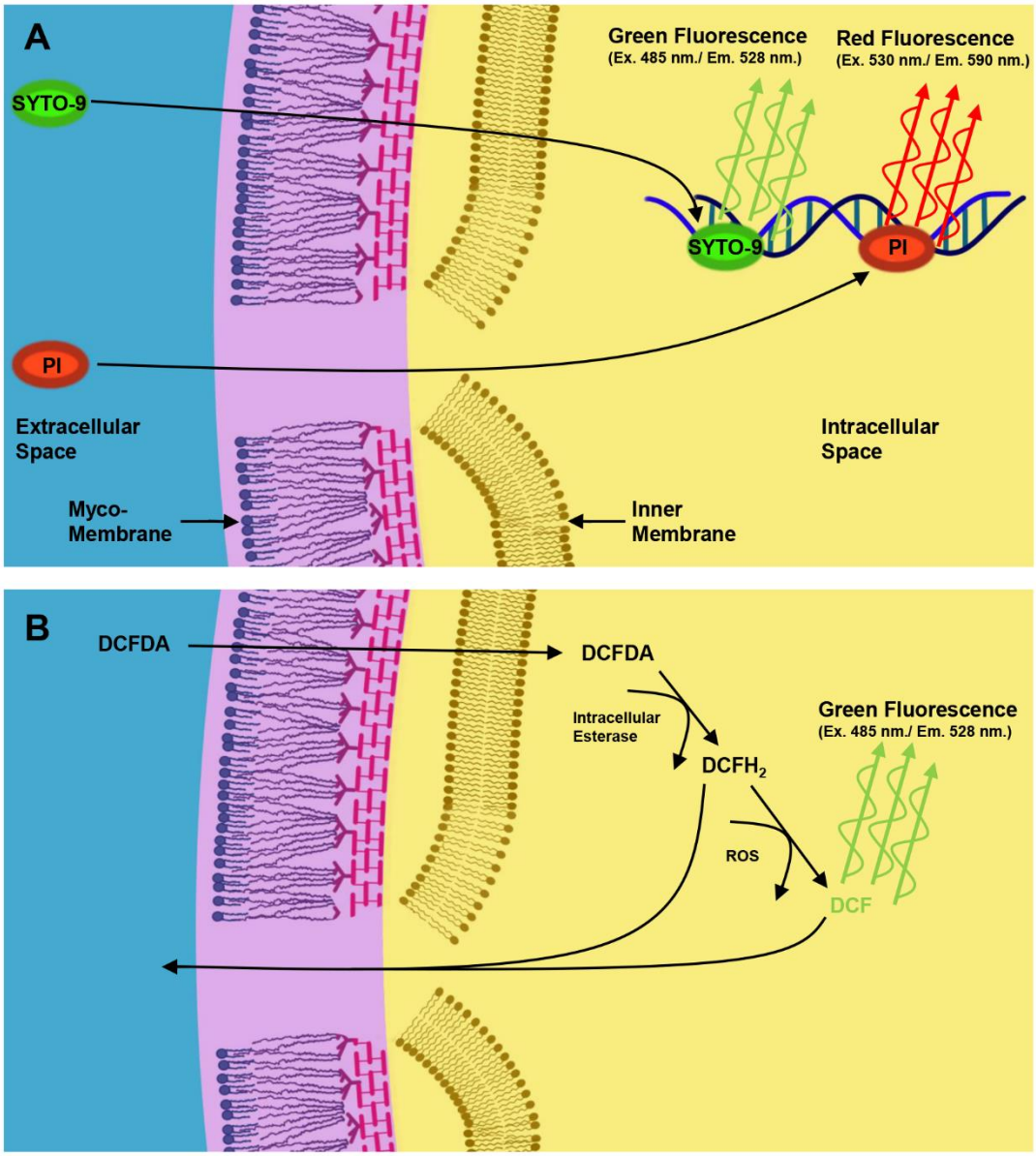

788

789